Separating physical and biological nutrient retention and quantifying uptake kinetics from ambient to saturation in successive mountain stream reaches

Timothy Covino,[1] Brian McGlynn,[1] and Michelle Baker[2]

Received 7 December 2009; revised 9 April 2010; accepted 29 April 2010; published 8 October 2010.

[1] Hydrological and biogeochemical processes in stream reaches impact the downstream transport of nutrients. The output from one stream reach becomes the input for the next, leading to serial processing along stream networks. The shape of the uptake-concentration curve for each reach indicates in-stream biological uptake of nutrient. Combined with physical retention due to hydrologic turnover, both biological and physical retention will control nutrient export downstream. We performed an instantaneous addition of conservative (chloride, Cl) and nonconservative nutrient (nitrate-nitrogen, NO_3-N) tracers to ascertain the relative roles of physical and biological retention across four adjacent reaches along a 3744 m stream network in the Sawtooth Mountains, ID. Physical retention dominated total retention ranging from 15% to 58% across individual reaches and totaling 81% across the entire stream length. Within each reach, biological uptake was strongly controlled by nutrient concentration. We quantified continuous Michaelis-Menten (M-M) kinetic curves for each reach and determined that ambient uptake (U_{amb}) ranged from 19 to 58 μg m^{-2} min^{-1}, maximum uptake (U_{max}) from 65 to 240 μg m^{-2} min^{-1}, and half-saturation constants (K_m) from 4.2 to 14.4 μg l^{-1} NO_3-N. Biological retention capacity indicated by U_{max} decreased in a downstream direction. Although biological retention capacity decreased moving downstream, it did not decrease as much as physical retention, which led to biological retention comprising a larger portion of total retention at downstream reaches. We suggest that accurate assessment of total retention across stream reaches and stream networks requires quantification of physical retention and the concentration-dependent nature of biological uptake.

Citation: Covino, T., B. McGlynn, and M. Baker (2010), Separating physical and biological nutrient retention and quantifying uptake kinetics from ambient to saturation in successive mountain stream reaches, *J. Geophys. Res.*, *115*, G04010, doi:10.1029/2009JG001263.

1. Introduction

[2] Quantifying nutrient export has been central to watershed biogeochemistry and hydrology since at least the 1960s [*Bormann and Likens*, 1967]. Hydrological and biogeochemical signals observed at watershed outlets integrate terrestrial and aquatic processes at the landscape scale. Separating these processes to determine the influence lotic systems can exert on nutrient retention has proven challenging. However, recent research has begun to highlight the role that streams and stream networks can play in controlling watershed nutrient export [e.g., *Alexander et al.*, 2000; *Bernhardt et al.*, 2005]. Stream network nutrient retention is composed of both physical (i.e., hydrologic exchange) and biological retention (i.e., biological uptake). Considerable research attention has focused on understanding the influence of in-stream biological uptake of nitrogen (N) on N retention at the stream reach scale (tens to hundreds of meters) [e.g., *Mulholland et al.*, 2008; *Mulholland et al.*, 2009; *Peterson et al.*, 2001; *Stream Solute Workshop*, 1990]. However, few studies have considered hydrologic exchange (i.e., physical retention) as important to nutrient export, characterized the influence of nutrient concentration on nutrient uptake efficiency, determined how these processes together influence downstream nutrient export, or expanded beyond the stream reach to the steam network scale.

[3] Hydrologic gains and losses to and from local groundwater have been found capable of resetting stream water chemistry and controlling stream water balances [*Covino and McGlynn*, 2007; *Payn et al.*, 2009]. These bidirectional exchanges of water between streams and local groundwater contribute to "hydrologic turnover" of stream water. This hydrologic turnover occurs as water lost from the stream is replaced by gains of different groundwater. This process of losing water with a particular solute signature and gaining

[1]Montana State University, Bozeman, Montana, USA.
[2]Utah State University, Logan, Utah, USA.

0148-0227/10/2009JG001263

water of a different solute signature has important implications for stream water chemistry, solute transport, and stream nutrient concentration inertia [*Brookshire et al.*, 2009].

[4] While hydrologic turnover can exert strong controls over watershed nutrient export dynamics, it has received little attention in the context of nutrient export and spiraling (but see *Triska et al.* [1989b]). Stream nutrient spiraling describes the simultaneous physical (i.e., transient storage) and biological (i.e., uptake) processes that control downstream transport of nutrients [*Newbold et al.*, 1981; *Newbold et al.*, 1983; *Webster and Patten*, 1979]. Typically, stream nutrient spiraling studies are based on recovered tracer only [*Stream Solute Workshop*, 1990]. As such, these analyses represent biological uptake of nutrient relative to recovered conservative tracer, which is important to overall watershed nutrient export but typically does not include the influence of hydrologic loss (i.e., physical retention) on nutrient export.

[5] Biological nutrient retention measured as uptake of a nonconservative nutrient tracer relative to a recovered conservative tracer is strongly influenced by stream nutrient concentrations. For example, *Mulholland et al.* [2002] found that uptake length (S_w) increased with elevated nutrient concentration, which indicated decreased nutrient use efficiency as nutrient concentration increased. Furthermore, *Mulholland et al.* [2008] noted that the nutrient export models that fail to incorporate the influence of concentration on uptake efficiency may be incorrect and might underestimate downstream export. This pattern is important because it suggests that biological retention efficiency decreases at those times when nutrient export can be highest [*Royer et al.*, 2004].

[6] The relationships between nutrient spiraling and concentration have been partially characterized for only a few stream reaches [*Earl et al.*, 2006]. This is in part due to the large effort, cost, and time required to develop spiraling-concentration curves using conventional methods [e.g., *Earl et al.*, 2006; *Stream Solute Workshop*, 1990]. However, a new method has been recently developed to characterize stream reach uptake kinetic curves quickly and relatively easily [*Covino et al.*, 2010]. This approach, tracer additions for spiraling curve characterization (TASCC), can provide full uptake kinetic curves for streams and quantification not only of ambient spiraling parameters but also of how they change in response to wide ranges in nutrient loading and concentrations [*Covino et al.*, 2010]. This method was developed in streams that are becoming rapidly nutrient enriched because of human development [*Covino et al.*, 2010]; however, here we apply the approach in a low-nutrient and non-human-impacted system. Furthermore, the ease with which rapid characterization of uptake kinetic curves (i.e., spiraling curves) can be obtained using this new dynamic TASCC method [*Covino et al.*, 2010] provides opportunity for repeat experiments to investigate how these kinetic curves change in response to changing environmental conditions (e.g., ambient concentration, biomass, temperature, light, etc.) through space and time [*Dent and Grimm*, 1999]. This is critical as we move from individual reaches to larger portions of the landscape to assess the role of the stream network in altering the timing and magnitude of nutrient export at the watershed scale.

[7] Application of the TASCC approach [*Covino et al.*, 2010] and characterization of nutrient spiraling curves from ambient to saturation can provide (1) ambient uptake lengths ($S_{w\text{-}amb}$), uptake velocities ($V_{f\text{-}amb}$), and areal uptake rates (U_{amb}); (2) maximum uptake rates (U_{max}); (3) half-saturation constants (K_m); and (4) stream system response to variable nutrient loading (i.e., buffering capacity, indicated by the trajectory of the uptake-concentration curves between U_{amb} and U_{max}). Many studies have measured or estimated ambient spiraling metrics for an individual stream reach, but none has fully characterized spiraling from ambient to saturation. While measures of ambient spiraling alone are important for understanding ambient conditions and links to other stream ecosystem processes such as metabolism [*Newbold et al.*, 2006], they gain increased power when considered in the context of U_{max} and K_m values. Measures of U_{max} and K_m can indicate stream nutrient uptake capacities and how a stream would likely respond to changing nutrient dynamics.

[8] Because the relationship between uptake efficiency and nutrient concentration exerts strong control over nutrient export and subsequent loading to downstream reaches and ecosystems, serial nutrient processing along stream networks will be closely linked to nutrient usage efficiency dynamics across the landscape. Considerations of ambient spiraling metrics alone, while valuable, only provide partial information and limit our ability to understand, quantify, and model the dynamics of nutrient uptake through space and time [*Mulholland et al.*, 2008].

[9] Accordingly, in this paper we quantify the physical, biological, and dynamic nature of nitrate-nitrogen (NO_3-N) retention across successive reaches along a 3744 m stream network in the Bull Trout Lake Watershed, Sawtooth Mountains, ID (Figure 1). These analyses begin to unravel the stream processes that partially control watershed nutrient export and the integrated biogeochemical and hydrological signals observed at watershed outlets. In this context, we address the following specific questions:

[10] 1. What are the relative contributions of physical and biological retention to total retention of N?

[11] 2. What influence does N concentration have on spiraling metrics and nutrient uptake efficiency?

[12] 3. How do these processes integrate to control network export?

2. Materials and Methods

2.1. Study Site

[13] We performed an instantaneous stream tracer addition on 14 June 2007 in the Bull Trout Lake Watershed (44.302961, −115.2564899), Sawtooth Mountains, ID (Figure 1). The watershed forms the headwaters of the Payette River drainage with an area of 11.71 km^2 and elevation range of 2117–2600 m. Valley bottom fill is composed of mixed Pleistocene till and Holocene alluvium and colluvium, and parent lithology is biotite granodiorite of the Idaho Batholith [*Kiilsgaard et al.*, 2003]. Thirty year average annual precipitation is 108 cm, 64% of which is snowfall, and 2007 annual precipitation totaled 95.8 cm (Banner Summit SNOwpack TELemetry, SNOTEL 312, 2140 m elevation located <2 km from Bull Trout). We

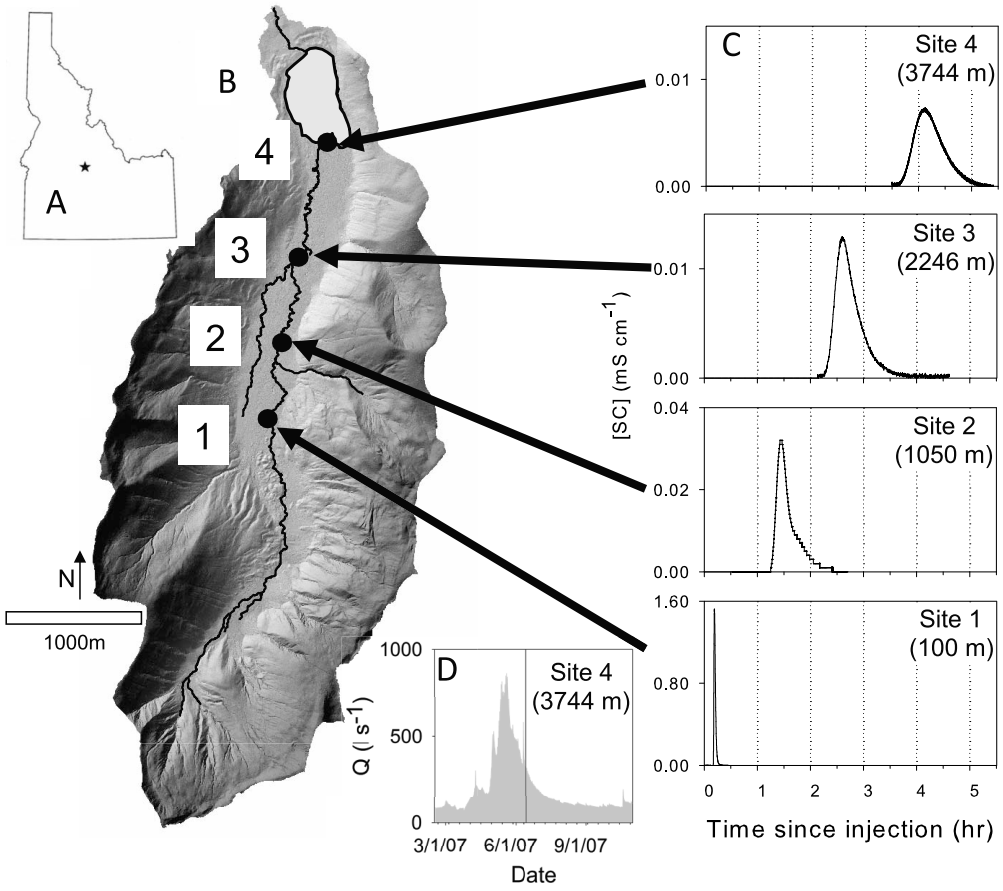

Figure 1. (a) Location of the Bull Trout Lake watershed in central Idaho, (b) detailed map of the 11.71 km^2 watershed including tracer test sampling locations, (c) specific conductivity of injected tracer breakthrough curves for each sampling location, and (d) annual hydrograph measured at site 4 (3744 m) with vertical line denoting timing of tracer test on 14 June 2007. Note the stream flows to the north and the different scales on *y* axes of breakthrough curves. Sites 1–4 are 100, 1050, 2246, and 3744 m from the injection site.

conducted our tracer addition over 3744 m of Spring Creek, which is the main channel draining the watershed and flows from south to north (Figure 1). Channel slopes ranged from 0.98% to 0.45%, and stream sinuosity was between 1.52 and 1.71 (Table 1). Stream discharge ranged between 197 and 328 L s^{-1} over the study reaches, with discharge increasing downstream, and water temperature ranged from 7.9°C to 10.4°C, also increasing downstream. Ambient NO_3-N concentrations were typical for the region [*Arp and Baker*, 2007], ranging from 4.1 to 7.4 μg L^{-1}. We injected tracer near the headwaters of the watershed and measured tracer concentrations over time (breakthrough curves (BTCs)) at four locations from the injection site to the inlet of Bull Trout Lake (Figure 1). Across the 3744 m study network, the stream trends from headwater stream and lodgepole pine (*Pinus contorta*) land cover, to valley bottom stream flowing through alluvial deposits and land cover dominated by sedges (*Carex* spp.), willows (*Salix* spp.), and grasses.

2.2. Instantaneous Addition of Cl and NO_3-N

[14] We dissolved 14.4 kg of conservative tracer (sodium chloride, NaCl) and 4.12 kg of nonconservative tracer

Table 1. Physical Characteristics Across Stream Reach Combinations

Stream Reach Combinations	Valley Distance (m)	Stream Distance (m)	Elevation Difference (m)	Valley Slope (%)	Stream Slope (%)	Wetted Width (m)	Stream Sinuosity
1–2	627	950	9.3 (2138.0–2128.7)	1.48	0.98	2.4	1.52
2–3	698	1196	6.2 (2128.7–2122.4)	0.89	0.52	4.8	1.71
3–4	954	1498	6.8 (2122.4–2115.6)	0.71	0.45	3.7	1.57

(potassium nitrate, KNO_3) in 200 L of stream water and introduced the solution to Spring Creek as an instantaneous addition (i.e., slug). We measured tracer BTCs real time (either Yellow Spring Instruments XLM minisonde, Yellow Springs, OH, or Campbell CS547A conductivity and temperature probes attached to CR1000 Campbell Scientific data loggers, Logan, UT; 1 or 2 s logging interval) at sampling locations 100 (site 1), 1050 (site 2), 2246 (site 3), and 3744 m (site 4) downstream of the injection site. We also collected streamwater grab samples across the BTCs at sites 2, 3, and 4. Water samples were field filtered through ashed 0.7 μm glass fiber filters (GF/F Whatman International, Ltd., Maidstone, UK), placed on ice and frozen until analysis. Upon return to the laboratory, Cl and NO_3-N in grab samples were analyzed on an ion chromatograph (Dionex Model 500, Sunnyvale, CA) with AS14A analytical and guard columns and a 500 μL injection loop.

2.3. Network Tracer Mass Recovery

[15] We used NaCl dilution gauging to determine local discharge at sites 1, 3, and 4, and discharge measurements made in this manner were conducted from the bottom of the stream network to the top over the course of a few hours prior to the combined Cl-NO_3-N addition. NaCl was administered to the stream as an instantaneous addition only far enough upstream of the sampling location to allow for complete mixing (35–50 m). Appropriate mixing lengths were determined via visual inspection of complete mixing of fluorescent Rhodamine-WT immediately preceding NaCl additions. Conductivity was measured real time (as above), and a linear relationship ($r^2 > 0.99$, $P < 0.0001$) between conductivity and NaCl concentration was used to calculate stream discharge. Using these data, we developed an area-discharge relationship to estimate discharge at site 2.

[16] We used these local discharge values to calculate mass recovery of injected tracers at each sampling site during the combined Cl-NO_3-N addition as the product of the time-integrated tracer concentration (from our grab samples) and the local discharge at each sampling location (equation 1).

$$T_{\mathrm{MR}} = Q \int_0^t T_{\mathrm{C}}(t)\mathrm{d}t, \tag{1}$$

where T_{MR} is the tracer mass recovered, T_{C} is the time-integrated tracer concentration, and Q is local stream discharge. From the tracer mass recovery, we calculated the mass loss (equation 2).

$$\text{Mass Loss} = \text{Mass Added} - T_{\mathrm{MR}}. \tag{2}$$

We used mass loss calculated in this way to partition NO_3-N tracer retention attributable to biological (i.e., uptake) versus physical (i.e., hydrologic loss) processes. Total tracer retention (TR) is defined as the amount of NO_3-N tracer we added that was not measured at a downstream sampling site (equation 3).

$$\mathrm{TR} = \text{Mass of } NO_3\text{-N added} - T_{\mathrm{MR}}(NO_3\text{-N}), \tag{3}$$

where "mass of NO_3-N added" is the total mass injected, and "$T_{\mathrm{MR}}(NO_3$-N)" is the mass of NO_3-N recovered at a downstream sampling site. Physical retention (PR) of NO_3-N was estimated proportionally from the Cl mass recovered (%) times the NO_3-N mass injected (equation 4):

$$\mathrm{PR} = (100 - T_{\mathrm{MR}}(\mathrm{Cl}\%) \times \text{Mass of } NO_3\text{-N added}, \tag{4}$$

where "T_{MR}(Cl%)" is the % of Cl added that was recovered. In-stream biological retention (BR) was calculated by difference (equation 5).

$$\mathrm{BR} = \mathrm{TR} - \mathrm{PR}. \tag{5}$$

In these calculations TR, PR, and BR are calculated as masses, which can then be easily converted into fractional or percent values.

[17] Our sampling extended through tracer breakthrough to background concentrations at all sites except for site 4 (3744 m) where we extrapolated to background. We determined the fractional mass recovery and therefore fractional mass loss for each tracer (NO_3-N and Cl) over each of the stream segments and across the entire 3744 m. To calculate the tracer loss over individual stream segments, we determined the mass of tracer recovered at site$_{(n)}$ compared to the tracer recovered at site$_{(n-1)}$.

2.4. Net Changes in Q, and Stream Gains and Losses

[18] From our discharge measurements, we determined the net discharge differences over our study reaches (equation 6):

$$\text{Net change in } Q = Q_{(\text{site } n)} - Q_{(\text{site } n\text{-}1)}, \tag{6}$$

where $Q_{(\text{site } n)}$ is Q at the downstream endpoint (i.e., base) of the stream reach and $Q_{(\text{site } n\text{-}1)}$ is Q at the upstream endpoint (i.e., head) of the stream reach. Although stream segments may be net gaining or net losing, they often both gain and lose water as they flow downstream [*Covino and McGlynn*, 2007]. Therefore, net changes in discharge are the result of gross stream water losses to and gains from groundwater over the stream reach (equation 7).

$$\text{Net change in } Q = \text{Gross Gain} - \text{Gross Loss}. \tag{7}$$

[19] The mass of conservative tracer loss approximates gross stream water losses over each stream reach within the network (e.g., we assumed 10% of conservative tracer loss approximately equals 10% stream water loss over the stream reach). We then rearranged equation 7 to solve for gross stream water gain (equation 8).

$$\text{Gross Gain} = \text{Net change in } Q + \text{Gross Loss}. \tag{8}$$

By solving this simple mass balance, we were able to estimate not only net changes in Q across each stream reach but also the gross losses and gains that combine to yield the net changes in Q.

2.5. BTC-Integrated Spiraling of Added NO_3-N ($S_{\text{w-add-int}}$, $V_{\text{f-add-int}}$, and $U_{\text{add-int}}$)

[20] Spiraling metrics estimated from nutrient addition experiments reflect the spiraling of added nutrient, not total nutrient spiraling. We used our combined Cl and NO_3-N addition to calculate added NO_3-N spiraling parameters. For each sampling site, we calculated the background-corrected

total mass recovery of Cl and NO_3-N using equation 1 and determined the NO_3-N:Cl ratio of those total mass recoveries (i.e., $T_{MR}(NO_3\text{-N}):T_{MR}(Cl)$. We then calculated BTC-integrated added nutrient uptake length ($S_{w\text{-}add\text{-}int}$) by regressing the natural log of the background corrected NO_3-N:Cl ratios against stream distance and taking the negative inverse of the slope of that line [*Ruggiero et al.*, 2006; *Tank et al.*, 2008] (equation 9):

$$S_{w\text{-}add\text{-}int} = -1/k_{w\text{-}add\text{-}int}, \tag{9}$$

where $k_{w\text{-}add\text{-}int}$ is the BTC-integrated longitudinal uptake rate of added nutrient and is equal to the slope of the least squares linear regression line [*Stream Solute Workshop*, 1990]. This calculation is of the same form as the exponential decay equation to calculate mean lifetime (equation 10):

$$\tau = 1/\lambda, \tag{10}$$

where τ is the mean lifetime of an element in a set (analogous to uptake length, S_w), and λ is the decay rate for that element (analogous to longitudinal uptake rate, k_w). Thus, in a space for time substitution, S_w is the mean distance that an element (NO_3-N in this case) travels in dissolved form in the water column. The mean distance traveled, or mean lifetime, of an element subject to exponential decay is the point at which 63% of the original mass has been lost and 37% of the original mass remains.

[21] We calculated the BTC-integrated uptake velocity of added nutrient ($V_{f\text{-}add\text{-}int}$) using equation 11:

$$V_{f\text{-}add\text{-}int} = Q/(wS_{w\text{-}add\text{-}int}), \tag{11}$$

where w is the average wetted stream width across the stream reach as measured with a meter tape at 9–15 cross sections. Lastly, we calculated the BTC-integrated streambed areal uptake rate of added NO_3-N ($U_{add\text{-}int}$) using equation 12.

$$U_{add\text{-}int} = V_{f\text{-}add\text{-}int}[NO_3\text{-}N_{add-int}]. \tag{12}$$

[22] The concentration term in equation 12 is the geometric mean of BTC-integrated conservative and observed NO_3-N concentrations (both background corrected) from all samples collected across the BTC (equation 13).

$$[NO_3\text{-}N_{add-int}] = \sqrt{\frac{Q\int_0^t [NO_3 - N_{add\text{-}obs}](t)dt}{\int_0^t Q(t)dt} * \frac{Q\int_0^t [NO_3\text{-}N_{cons}](t)dt}{\int_0^t Q(t)dt}}, \tag{13}$$

where "NO_3-$N_{add\text{-}obs}$" is the background-corrected observed NO_3-N concentrations in the grab samples and "NO_3-N_{cons}" is the conservative NO_3-N concentrations. We defined conservative NO_3-N as the NO_3-N expected at a site if NO_3-N traveled conservatively (i.e., no uptake, maximum NO_3-N that could arrive at a site) and calculated conservative NO_3-N as the background-corrected Cl concentration times the ratio of NO_3-N:Cl in the injection solution. Similar to our "conservative" NO_3-N term, other studies have used the term "expected" [e.g., *Brookshire et al.*, 2005; *Ruggiero et al.*, 2006] or "predicted" [*Baker et al.*, 1999] in reference to conservative nutrient transport. The geometric mean of observed and conservative NO_3-N used in equation 12 (and other analyses) represents an averaging of nutrient that arrived (observed) and the maximum that could have arrived (conservative) at the sampling stations. We believe this provides a good approximation of the NO_3-N concentration experienced over the stream segment of interest (i.e., the concentration experienced across the reach is greater than observed values). Further, the geometric mean has previously been used to "average" longitudinal solute concentrations during stream tracer experiments [e.g., *Payn et al.*, 2005; *Earl et al.*, 2006]. We completed our analyses using both the geometric and arithmetic means, and the results were indistinguishable; we chose to use the geometric mean in order to be consistent with prior studies.

2.6. Dynamic Spiraling of Added NO_3-N ($S_{w\text{-}add\text{-}dyn}$, $V_{f\text{-}add\text{-}dyn}$, and $U_{add\text{-}dyn}$)

[23] In contrast to the BTC-integrated approach to spiraling as described above, the BTC data present an opportunity to evaluate how biological uptake responds in a dynamic way to variable NO_3-N concentration [*Covino et al.*, 2010]. The BTC-integrated approach collapses all the grab sample data into one value, whereas with the dynamic TASCC method spiraling values are obtained for each grab sample and spiraling metric versus concentration curves can be developed. We calculated dynamic spiraling parameters for each data point in the BTCs collected at each of three sampling sites. First, we calculated dynamic uptake length ($S_{w\text{-}add\text{-}dyn}$) by plotting the background-corrected NO_3-N:Cl ratios of injectate and each BTC grab sample against stream distance from the injection site to each of the three downstream sampling stations using instantaneous concentrations, not integrated masses as described above. The slopes of the lines fit to those data are the dynamic longitudinal uptake rates ($k_{w\text{-}add\text{-}dyn}$) and the negative inverse of those slopes are $S_{w\text{-}add\text{-}dyn}$ (equation 14).

$$S_{w\text{-}add\text{-}dyn} = -1/k_{w\text{-}add\text{-}dyn}, \tag{14}$$

where $S_{w\text{-}add\text{-}dyn}$ is the dynamic added nutrient uptake length and $k_{w\text{-}add\text{-}dyn}$ is the dynamic longitudinal uptake rate. We then applied equations 15 and 16 to calculate dynamic uptake velocity ($V_{f\text{-}add\text{-}dyn}$) and dynamic areal uptake rate ($U_{add\text{-}dyn}$) for each of the BTCs' grab samples.

$$V_{f\text{-}add\text{-}dyn} = Q/(wS_{w\text{-}add\text{-}dyn}) \tag{15}$$

$$U_{add\text{-}dyn} = V_{f\text{-}add\text{-}dyn}[NO_3\text{-}N_{add\text{-}dyn}] \tag{16}$$

[24] In these equations, $V_{f\text{-}add\text{-}dyn}$ is the dynamic uptake velocity, and $U_{add\text{-}dyn}$ is the dynamic areal uptake rate of added nutrient. The concentration term in equation 16 is the geometric mean of conservative and observed instantaneous NO_3-N concentrations for each individual grab sample (not integrated as above in equations 12 and 13). We also calculated dynamic areal uptake for each grab sample using a mass balance approach (equation 17):

$$U_{add\text{-}dyn\text{-}MB} = ([NO_3\text{-}N_{cons}] - [NO_3\text{-}N_{add\text{-}obs}])Q/(\text{streambed area}), \tag{17}$$

where $U_{add\text{-}dyn\text{-}MB}$ is the mass balance–calculated dynamic

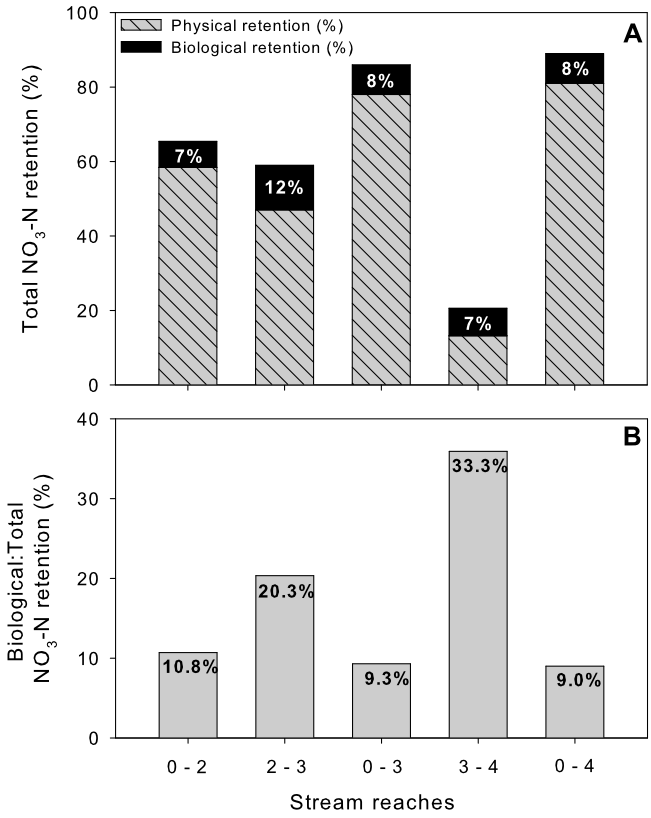

Figure 2. (a) Total NO_3-N retention across stream reaches separated into physical and biological components. The total height of the bar is equal to the total NO_3-N retention across the reach, the black portion of the bar represents NO_3-N retention attributable to biological processes (uptake), and the gray-hatched portion of the bar represents NO_3-N retention attributable to physical processes (hydrologic loss). The values in the black portion of the bars are the percentages of biological retention over that stream segment. We define retention as added tracer that was not recovered at a downstream sampling site. (b) The proportion of total retention attributable to biological retention (i.e., biological retention divided by total retention) for our different stream reach combinations. The black numbers equal the magnitude of biological proportional retention.

areal uptake rate of added nutrient, NO_3-N_{cons} is the expected instantaneous NO_3-N concentration in the grab sample of interest if NO_3-N traveled conservatively, NO_3-$N_{add\text{-}obs}$ is the background-corrected observed instantaneous NO_3-N concentration in the grab sample of interest, and streambed area is the average streambed area across the stream reach calculated as the product of stream length and the average wetted width across the reach.

2.7. Ambient and Total Spiraling Metrics and Kinetic Model Parameterization

[25] We used the methods outlined in *Covino et al.* [2010] to estimate ambient uptake length ($S_{w\text{-}amb}$). In this method, uptake length is plotted against nutrient concentration and a linear regression is then fit to these data. That relationship is then used to back extrapolate to lower nutrient concentration values than those of the nutrient addition experiments, thus, estimating $S_{w\text{-}amb}$. From our $S_{w\text{-}amb}$ estimates, we calculated ambient areal uptake (U_{amb}) and uptake velocity ($V_{f\text{-}amb}$) (equations 18 and 19):

$$U_{amb} = (Q[NO_3\text{-}N_{amb}])/(S_{w-amb}w) \quad (18)$$

$$V_{f-amb} = U_{amb}/[NO_3\text{-}N_{amb}], \quad (19)$$

where $[NO_3$-$N_{amb}]$ is the ambient stream NO_3-N concentration (i.e., concentration without influence of nutrient addition). During nutrient addition experiments total stream areal nutrient uptake (U_{tot}) is equal to the sum of the uptake of added and ambient nutrient. By combining our added and ambient uptake values, we estimated total uptake rates for both BTC-integrated and dynamic TASCC methods (equations 20 and 21):

$$U_{tot\text{-}int} = U_{add\text{-}int} + U_{amb} \quad (20)$$

$$U_{tot\text{-}dyn} = U_{add\text{-}dyn} + U_{amb}, \quad (21)$$

where $U_{tot\text{-}int}$ is the BTC-integrated total areal uptake rate and $U_{tot\text{-}dyn}$ is the dynamic total areal uptake for each grab sample (note, $U_{add\text{-}dyn}$ can be calculated using either the mass-balance approach (equation 17) or using the Stream Solute Workshop approach (equation 16), discussed in a later section). Total uptake velocities ($V_{f\text{-}tot}$) for BTC-integrated and dynamic methods were calculated as (equations 22 and 23):

$$V_{f\text{-}tot\text{-}int} = U_{tot\text{-}int}/[NO_3\text{-}N_{tot\text{-}int}] \quad (22)$$

$$V_{f\text{-}tot\text{-}dyn} = U_{tot\text{-}dyn}/\left[NO_3\text{-}N_{tot\text{-}dyn}\right] \quad (23)$$

where $V_{f\text{-}tot\text{-}int}$ is the BTC-integrated total uptake velocity,

Table 2. Summary of Physical and Biological Retention of NO_3-N Across the Stream Reach Combinations[a]

Stream Reach Combinations	Distance (m)	Physical Retention (%)	Biological Retention (%)	Total Retention (%)	Physical Retention (% 100 m^{-1})	Biological Retention (% 100 m^{-1})	Total Retention (% 100 m^{-1})	$k_{w\text{-}add\text{-}int}$ (m^{-1})
0–2	1050	58	7	65	5.56	0.67	6.23	-2.72×10^{-4}
2–3	1196	47	12	59	3.93	1.00	4.93	-1.33×10^{-4}
0–3	2246	78	8	86	3.47	0.36	3.83	-1.98×10^{-4}
3–4	1498	13	7	21	0.88	0.49	1.38	-5.92×10^{-5}
0–4	3744	81	12	89	2.16	0.21	2.38	-1.42×10^{-4}

[a]We show the bulk retention across each reach combination (left side of table) and normalized to retention per 100 m of stream reach (right side of table). We also give the BTC-integrated added nutrient longitudinal uptake rates ($k_{w\text{-}add\text{-}int}$) for each reach combination. We define retention as added NO_3-N that was not exported in stream flow past a sampling site.

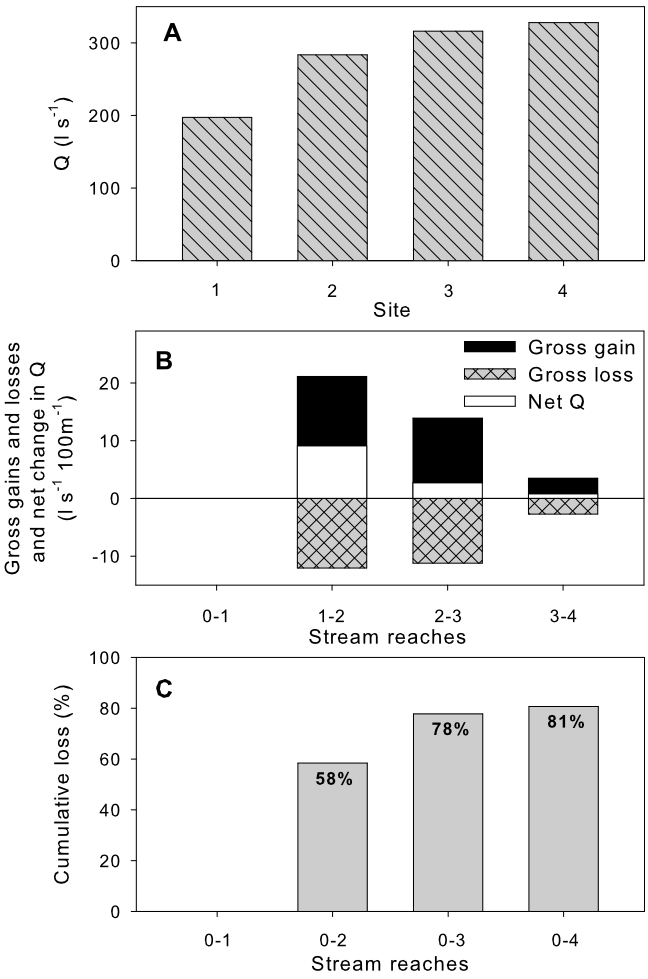

Figure 3. (a) Stream discharge (Q) at sites 1 (100 m), 2 (1050 m), 3 (2246 m), and 4 (3744 m); (b) gross gains, losses, and net change in Q per 100 m of stream length between sites 1 and 2, 2 and 3, and 3 and 4. Gross gains and losses are defined as the gross gain from groundwater and gross loss to groundwater that sum to equal net changes in discharge over each reach. (c) Cumulative % hydrologic loss between sites 0 and 2, 0 and 3, and 0 and 4. Cumulative % hydrologic loss totaled 81% over the 3744 m of stream even though there was net gain in Q of 131 L s^{-1}.

$[NO_3\text{-}N_{tot\text{-}int}]$ is the geometric mean of BTC-integrated conservative and total observed NO_3-N (i.e., not background corrected) concentrations from all grab samples across the BTC, $V_{f\text{-}tot\text{-}dyn}$ is the dynamic total uptake velocity, and $[NO_3\text{-}N_{tot\text{-}dyn}]$ is the geometric mean of conservative and total observed NO_3-N (i.e., not background corrected) concentrations in the grab sample of interest. From the dynamic analyses, we developed spiraling metric versus nutrient concentration curves, which are useful, among other things, for assigning appropriate kinetic models and kinetic model parameterization. We fit the Michaelis-Menten (M-M) model (equation 24)

$$U = \frac{U_{max} C}{K_m + C} \tag{24}$$

to our $U_{tot\text{-}dyn}$ data (SigmaPlot, SPSS, Chicago, IL, USA) to estimate maximum uptake (U_{max}) and the half-saturation constant (K_m) (C is the geometric mean of conservative and total observed nutrient concentration). It is important to use total spiraling parameters when fitting the M-M equation, or other kinetic models, to uptake data because parameter estimates based on spiraling of added nutrient alone would be incorrect. The magnitude and direction of errors in these incorrect U_{max} and K_m estimates gleaned from added nutrient spiraling data alone are dependent on the relationship between U_{amb} and ambient nutrient concentration [*Covino et al.*, 2010]. Also, the dynamic analyses provide complete characterization of spiraling metric versus concentration curves, whereas the BTC-integrated approach yields only one data point on the greater spiraling metric-concentration curve.

3. Results

3.1. Physical and Biological Retention of NO_3-N

[26] Over the 3744 m study stream network, physical retention comprised 81% and biological retention comprised 8% of total NO_3-N retention (note biological retention refers to in-stream biological nutrient uptake, and we define retention as added tracer that was not exported in stream flow past a sampling site) (Figure 2a and Table 2). The total amount of NO_3-N tracer retention was 89%, while 11% of the added tracer was exported beyond our study area. Biological retention was greatest between sampling sites 2 and 3 at 12% and was 7%–8% of total NO_3-N retention across our other stream reach combinations (Figure 2a and Table 2). Physical retention of tracer decreased moving downstream from 58% between sites 0 and 2 to 13% between sites 3 and 4 (Table 2). Total retention also decreased moving downstream, largely driven by the physical retention pattern observed along the stream network (Figure 2 and Table 2). The decreases in physical retention were not accompanied by equivalent decreases in biological retention in a downstream direction. This led to biological retention becoming a

Table 3. Summary of Hydrologic Dynamics Across Stream Reach Combinations[a]

Stream Reach Combinations	Watershed Area (km^2)	Distance (m)	Q (L s^{-1})	Net Q (L s^{-1} 100 m^{-1})	Gross Gain (L s^{-1} 100 m^{-1})	Gross Loss (L s^{-1} 100 m^{-1})	Median Flow Velocity (m s^{-1})
0–1	3.9	100	197	NA	NA	NA	0.214
1–2	7.5	950	284	9.1	21.1	−12.0	0.190
2–3	9.0	1196	316	2.7	13.9	−11.2	0.231
3–4	10.8	1498	328	0.8	3.5	−2.7	0.247

[a]Site 1 is the upstream boundary condition and as such net change in Q, gross gain, and gross loss do not apply at this site (indicated by NA).

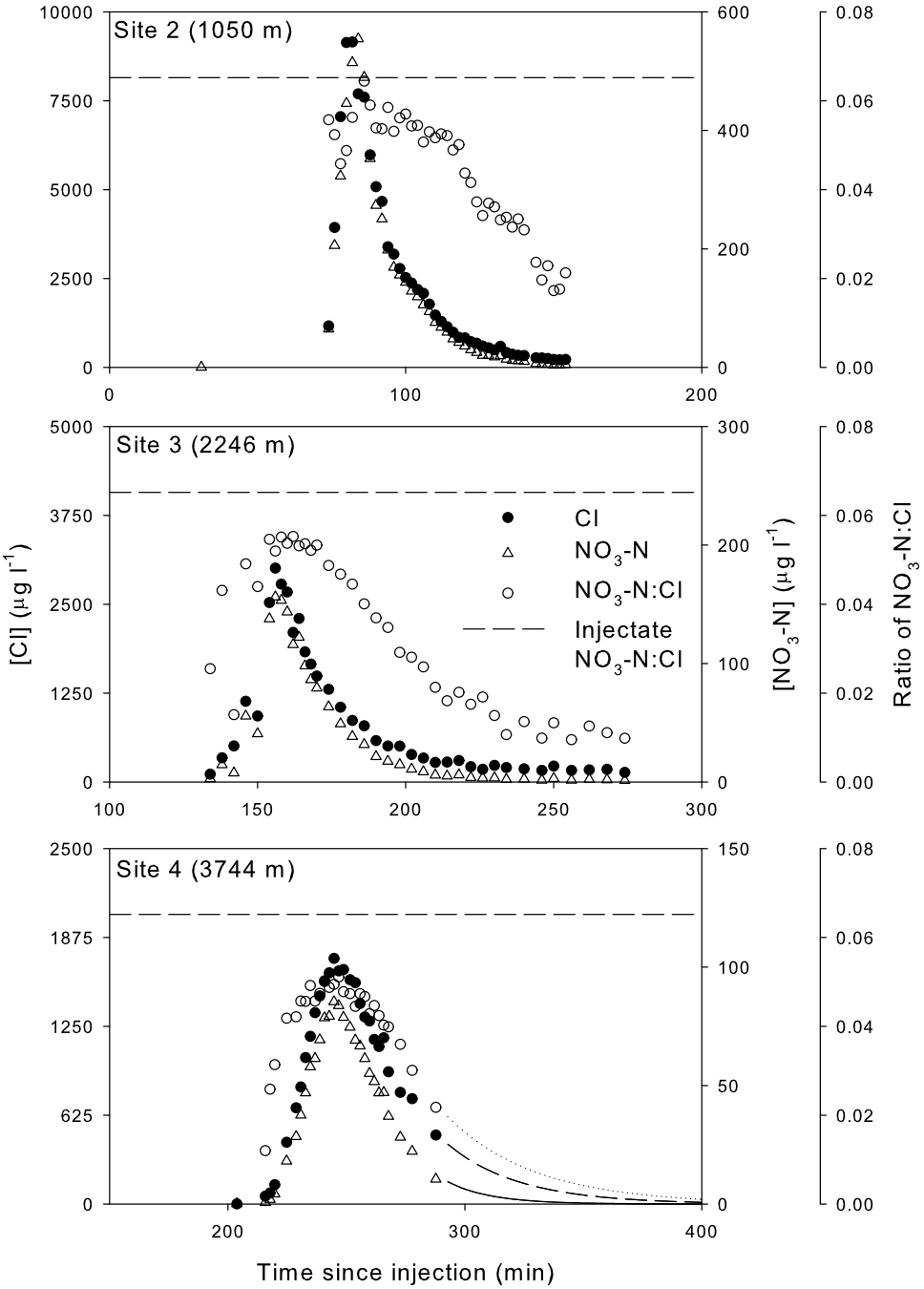

Figure 4. Time series of Cl, NO_3-N, and the ratio of NO_3-N:Cl at each site. The changing ratios of NO_3-N:Cl indicate times of greater and lesser NO_3-N uptake across the breakthrough curves. The injectate NO_3-N:Cl ratio is shown for reference, indicated by the dashed line that is equal to 0.0652. We extrapolated the falling limb at site 4 (3744 m) to background with an exponential decay fit to falling limb grab samples, indicated by the lines extending from the grab sample breakthrough curves.

larger proportion of total retention at downstream reaches (Figure 2b). The ratio of biological-total retention was greatest between sites 3 and 4 at 33.3% (i.e., biological retention divided by total retention equaled 33.3%) and was only 10.8% between sites 0 and 2 (Figure 2b and Table 2). However, at the stream network scale, physical retention was dominant; over the 3744 m (sites 0–4), the biological-total retention ratio was 9% (Figure 2b).

3.2. Net Changes in *Q* and Gross Losses and Gains

[27] Despite recovery of only 19% of added Cl at the bottom of the stream network, total discharge (Q) increased moving downstream from 197 l s^{-1} at site 1 (100 m), 284 l s^{-1} at site 2 (1050 m), 316 l s^{-1} at site 3 (2246 m), and 328 l s^{-1} at

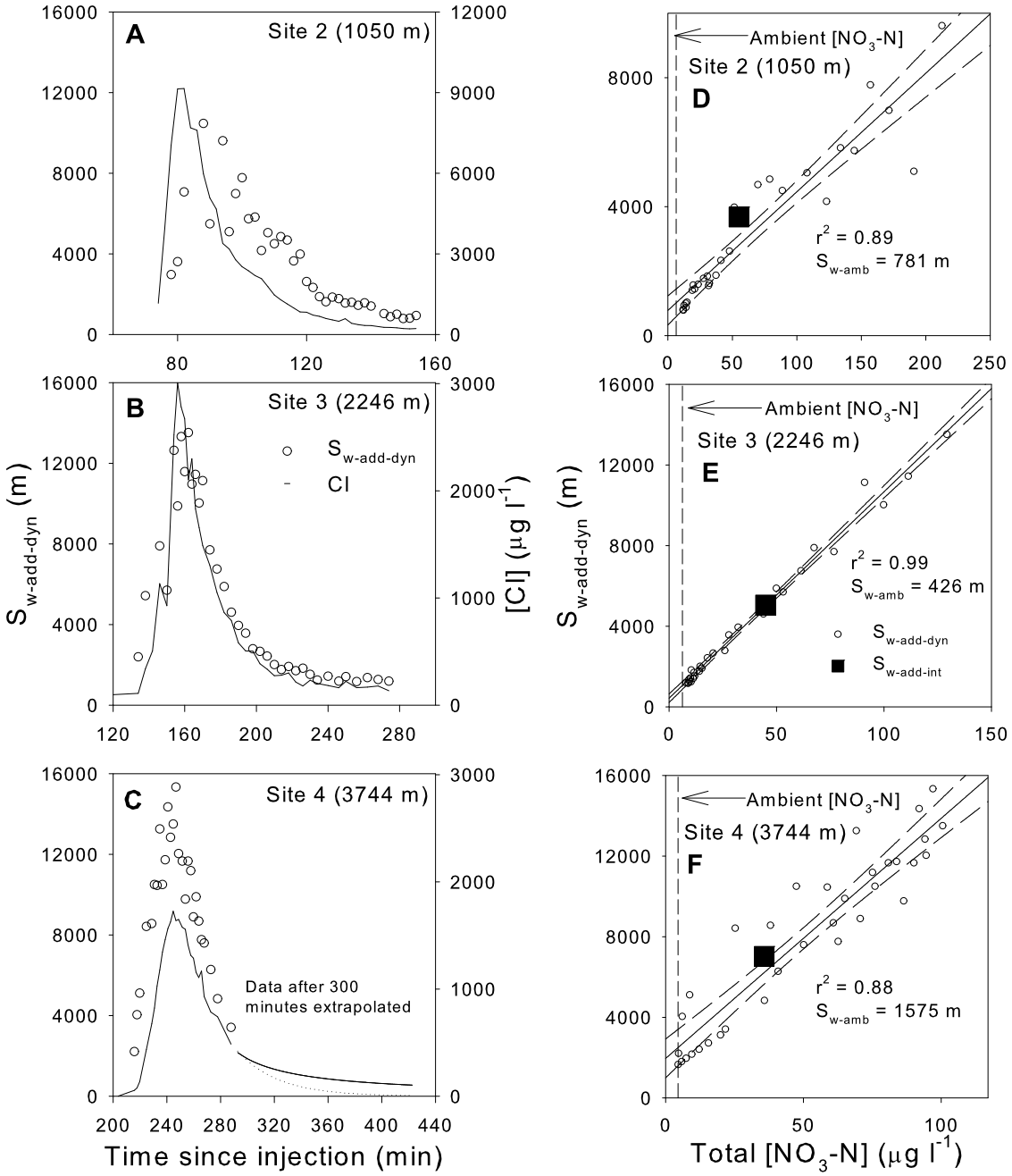

Figure 5. (a–c) Time series of added nutrient dynamic uptake length ($S_{w\text{-}add\text{-}dyn}$) and Cl breakthrough curves (BTCs) at sites 2 (1050 m), 3 (2246 m), and 4 (3744 m). Time axes are time since start of injection, and Cl grab sample values are shown as a solid line for clarity. (d–f) Linear regressions of $S_{w\text{-}add\text{-}dyn}$ versus total [NO_3-N] to estimate ambient uptake lengths ($S_{w\text{-}amb}$). Total [NO_3-N] is the geometric mean of conservative and observed total NO_3-N concentration.

site 4 (3744 m) (Figure 3a and Table 3). Gross losses and gross gains were observed over each of these net gaining stream reaches (Figure 3b). We determined the gross gains and losses and net changes in Q between sites and normalized these values for stream distance (i.e., values are per 100 m of stream length). In these between-site analyses, the Q and tracer mass recovered (T_{MR}) at site 2 become the input for site 3 and so on. Between sites 1 and 2 (100 and 1050 m), there were gross losses of −12.0, gross gains of +21.1, and a +9.1 l s^{-1} 100 m^{-1} change in net Q; between sites 2 and 3 (1050 and 2246 m), there were gross losses of −11.2, gross gains of +13.9, and a net change of +2.7 l s^{-1} 100 m^{-1}; and between sites 3 and 4 (2246 and 3744 m), there were gross losses of −2.7, gross gains of +3.5, and a net change of +0.8 l s^{-1} 100 m^{-1} (Figure 3b and Table 3). Cumulative gross losses were 58% between sites 0 and 2, 78% between sites 0 and 3, and 81% over the entire 3744 m (sites 0 and 4) (Figure 3c).

Table 4. Summary of Ambient Uptake Parameters[a]

Site	Average ambient stream $[NO_3\text{-}N]$ (μg L^{-1})	$S_{w\text{-}amb}$ (m)	$V_{f\text{-}amb}$ (mm min^{-1})	U_{amb} (μg m^{-2} min^{-1})	U_{max} (μg m^{-2} min^{-1})	K_m (μg L^{-1})	r^2
2	6.43	781	9.1	58	240	13.8	0.66
3	6.22	426	9.3	58	104	4.2	0.74
4	5.59	1575	3.4	19	65	14.4	0.78

[a]Ambient uptake length ($S_{w\text{-}amb}$), uptake velocity ($V_{f\text{-}amb}$), and areal uptake rate (U_{amb}) along with Michaelis-Menten (M-M) parameter values maximum uptake (U_{max}) and half-saturation constant (K_m). Coefficient of determination (r^2) values refer to the goodness of fit of the M-M equation to the uptake-concentration curve data in Figure 7.

3.3. BTC NO_3-N, Cl, and NO_3-N:Cl Ratios

[28] Aside from use to account for tracer dilution, the ratio of NO_3-N:Cl provides insight into nitrate uptake at each location as a function of concentration. If both of these tracers were traveling conservatively, at each measurement location, the ratio of the two should not change over time and should match the injectate ratio (0.0652; Figure 4, dashed line). Lower ratios of NO_3-N relative to Cl indicate more uptake of NO_3-N compared to samples with a higher ratio when NO_3-N is being transported more conservatively (e.g., near BTC peak). The time series BTCs of the NO_3-N/Cl ratio vary at each site (Figure 4), illustrating times of greater and lesser NO_3-N uptake. At site 2 (1050 m), the ratio of NO_3-N/Cl begins near 0.05, rises slightly and approaches the injectate ratio of 0.0652 near the BTC peak, and then falls to values near 0.02 on the falling limb tail of the BTC (Figure 4). At site 3 (2246 m), the ratio begins near 0.02, rises to values near 0.06 at the peak of the BTC, and then falls to values below 0.02 on the tail of the falling limb. There is a similar pattern at site 4 (3744 m) with values near 0.02 at the leading edge of the BTC, a rise to values near 0.05 at the peak of the BTC, and a fall to values near 0.02 on the tail of the falling limb (which we subsequently extrapolated to background) (Figure 4). These data were used to calculate the dynamic and BTC-integrated spiraling parameters.

3.4. Uptake Length and Ambient Nutrient Spiraling Parameters

[29] On the basis of the data described above, we calculated added nutrient dynamic uptake lengths ($S_{w\text{-}add\text{-}dyn}$) for each of the grab samples at sampling sites 2, 3, and 4 and BTC-

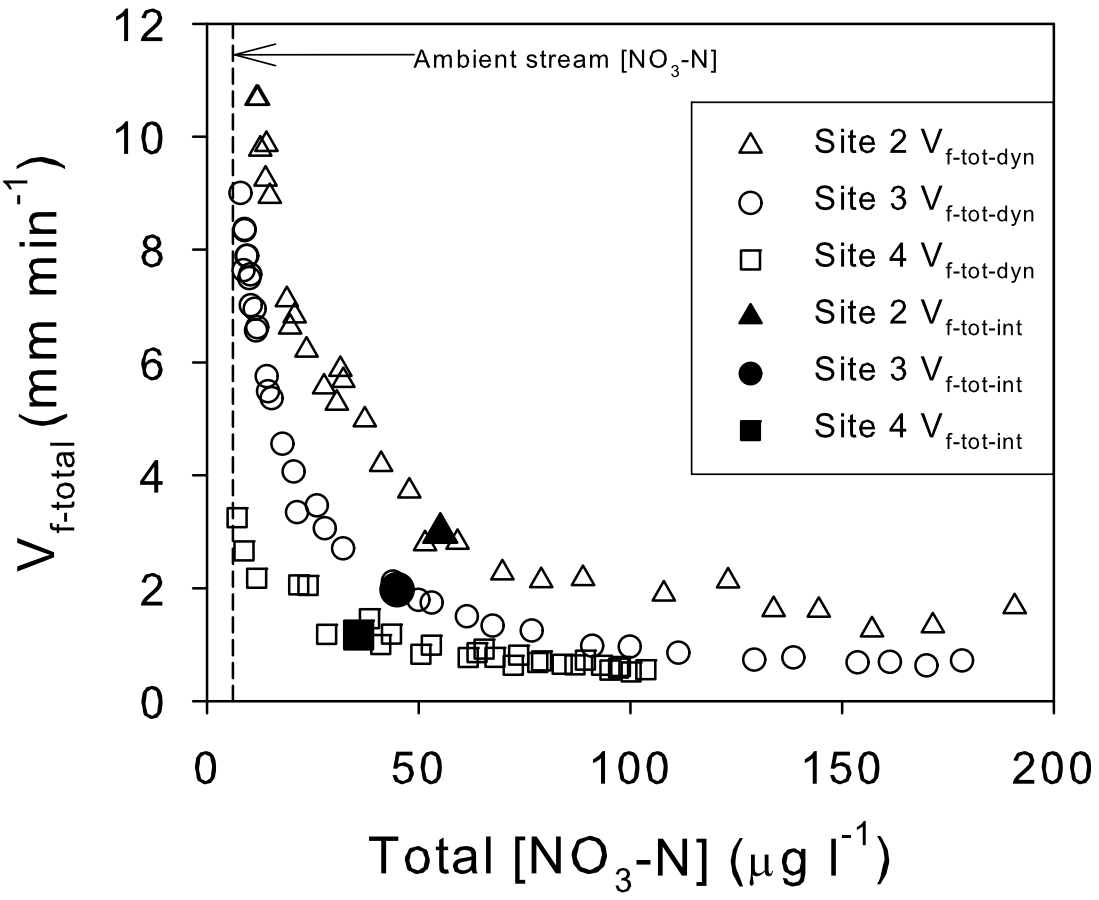

Figure 6. Dynamic total uptake velocity ($V_{f\text{-}tot\text{-}dyn}$) and BTC-integrated total uptake velocity ($V_{f\text{-}tot\text{-}int}$) versus the geometric mean of conservative and observed total NO_3-N concentration for sites 2, 3, and 4.

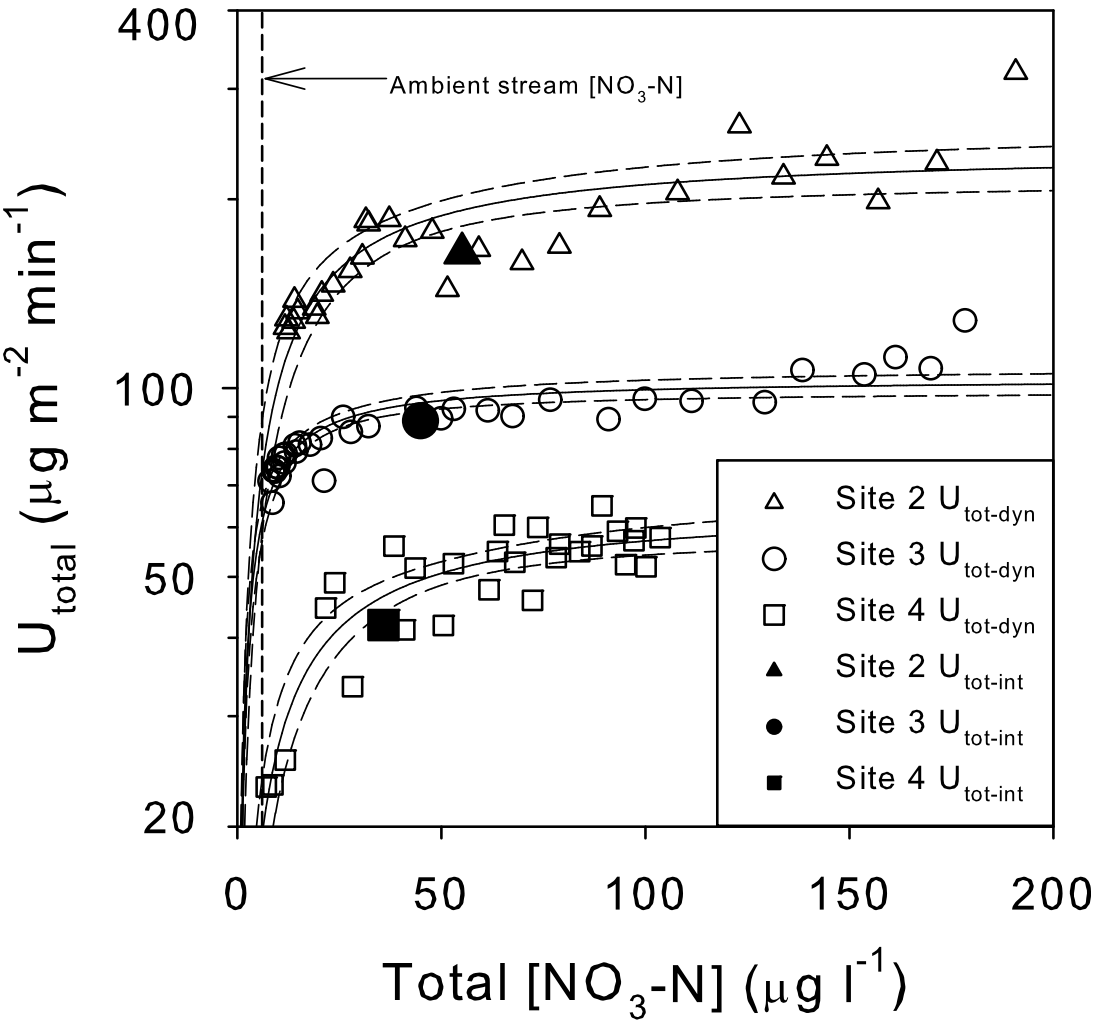

Figure 7. (a) Total dynamic areal uptake ($U_{tot\text{-}dyn}$) and BTC-integrated total areal uptake ($U_{tot\text{-}int}$) versus the geometric mean of conservative and observed total NO_3-N concentration for sites 2, 3, and 4.

integrated uptake lengths ($S_{w\text{-}add\text{-}int}$) for sites 2, 3, and 4 (Figure 5). At site 2, dynamic uptake length ($S_{w\text{-}add\text{-}dyn}$) began at a value near 3000 m, rose to a peak of 10,500 m, and fell again to values near 1000 m (Figure 5a). Site 3 $S_{w\text{-}add\text{-}dyn}$ values began near 2400 m, rose to a value of 13,500 m, and fell to values near 1200 m (Figure 5b). At site 4, $S_{w\text{-}add\text{-}dyn}$ began at 2200 m, rose to a peak of 15,300 m, and fell to a value of 3410 m, which we then extrapolated to values near 1000 m (Figure 5c). The $S_{w\text{-}add\text{-}int}$ values were 3678 m at site 2, 5055 m at site 3, and 7022 m at site 4 (Figures 5d–5f). The $S_{w\text{-}add\text{-}int}$ for the whole stream reach, calculated using NO_3-N/Cl ratios at sites 0, 2, 3, and 4 versus distance downstream, was 7262 m.

[30] $S_{w\text{-}add\text{-}dyn}$ increased linearly with concentration at each of the sampling sites, and we used these relationships to estimate ambient uptake lengths ($S_{w\text{-}amb}$) for each stream reach (Figures 5d–5f) [*Payn et al.*, 2005]. Ambient uptake lengths were 781 m at site 2, 426 m at site 3, and 1575 m at site 4 (Figure 5 and Table 4). The relationships between $S_{w\text{-}add\text{-}dyn}$ and NO_3-N concentration were based on 30 data points at site 2, 29 at site 3, and 34 at site 4, which are far greater than the two to three data points typically used in this type of ambient estimation (Figure 5). The coefficients of determination (r^2) for these relationships were 0.89 at site 2, 0.99 at site 3, and 0.88 at site 4 (Figure 5). From the $S_{w\text{-}amb}$ estimates, we also estimated ambient areal uptake (U_{amb}) and ambient uptake velocity ($V_{f\text{-}amb}$) for each site. The U_{amb} values were 58 at site 2, 58 at site 3, and 19 μg m^{-2} min^{-1} at site 4 (Table 4). Ambient uptake velocities were 9.1 at site 2, 9.3 at site 3, and 3.4 mm min^{-1} at site 4 (Table 4).

3.5. Total Nutrient Spiraling Parameters and the Influence of Nutrient Concentration

[31] As previously mentioned, total nutrient spiraling during an addition experiment reflects the spiraling ambient and added nutrient. Accordingly, we combined our ambient and added nutrient spiraling measurements to investigate the relationships between stream NO_3-N concentration and total dynamic uptake velocity ($V_{f\text{-}tot\text{-}dyn}$) and total dynamic areal uptake ($U_{tot\text{-}dyn}$) in order to characterize stream response to variable nutrient concentration. Both the $V_{f\text{-}tot\text{-}dyn}$ and $U_{tot\text{-}dyn}$ data followed M-M kinetics. First, we observed a negative exponential decay in $V_{f\text{-}tot\text{-}dyn}$ as a function of total NO_3-N concentration for each of the three sites (Figure 6). Site 2 generally had the highest $V_{f\text{-}tot\text{-}dyn}$ as a function of concentration, followed by site 3 and then site 4 (Figure 6). This

implies that sites 3 and 4 have a lower uptake velocity for a given NO_3-N concentration compared to site 2. The slope of the $V_{f\text{-}tot\text{-}dyn}$ versus NO_3-N concentration curve changed sharply between NO_3-N concentrations of ~5 $\mu g\ L^{-1}$ to ~100 $\mu g\ L^{-1}$ (Figure 6). At NO_3-N concentrations greater than ~100 $\mu g\ L^{-1}$, $V_{f\text{-}tot\text{-}dyn}$ stabilized at 2 mm min^{-1} for site 2 and ~0.5 mm min^{-1} for sites 3 and 4 (Figure 6). In the context of these dynamic estimates, the BTC-integrated uptake velocities ($V_{f\text{-}tot\text{-}int}$) were near the low $V_{f\text{-}tot\text{-}dyn}$ values, which indicates decreased nutrient use efficiency at these concentrations (36–55 $\mu g\ L^{-1}$ NO_3-N) (Figure 6). At site 2, $V_{f\text{-}tot\text{-}int}$ was 2.98; at site 3, $V_{f\text{-}tot\text{-}int}$ was 1.97; and at site 4, $V_{f\text{-}tot\text{-}int}$ was 1.17 mm min^{-1} (Figure 6). These BTC-integrated values compress the dynamic data into a single spiraling measurement and represent one point within the greater relationship between spiraling and nutrient concentration.

[32] The relationship between $U_{tot\text{-}dyn}$ and concentration was hyperbolic, indicative of M-M kinetics (Figure 7). We only display and discuss the $U_{tot\text{-}dyn}$ values calculated using the mass-balance approach because regression analysis shows that the two approaches (equations 16 and 17) produce identical estimates of added nutrient uptake ($U_{add\text{-}dyn}$ versus $U_{add\text{-}dyn\text{-}MB}$ ($r^2 > 0.99$, $P < 0.0001$), and therefore, either of these approaches give the exact same values of $U_{tot\text{-}dyn}$ (see equation 21). For each sampling site, there was an asymptotic rise toward maximum total uptake (U_{max}) at increased NO_3-N concentrations (Figure 7). For a given NO_3-N concentration, $U_{tot\text{-}dyn}$ was greatest at site 2, followed by site 3, and then site 4 (Figure 7). Site 2 $U_{tot\text{-}dyn}$ began at ~125 and rose to maximum values of ~250–300 $\mu g\ m^{-2}\ min^{-1}$, site 3 $U_{tot\text{-}dyn}$ began at ~65 and rose to maximum values of ~100 $\mu g\ m^{-2}\ min^{-1}$, and site 4 $U_{tot\text{-}dyn}$ began at ~20 and rose to maximum values of ~60 $\mu g\ m^{-2}\ min^{-1}$ (Figure 7). The BTC-integrated total uptake values ($U_{tot\text{-}int}$) fell in the middle to upper range of the $U_{tot\text{-}dyn}$ versus concentration curves and were 164 $\mu g\ m^{-2}\ min^{-1}$ at site 2, 89 $\mu g\ m^{-2}\ min^{-1}$ at site 3, and 42 $\mu g\ m^{-2}\ min^{-1}$ at site 4 (Figure 7). As with the BTC-integrated $V_{f\text{-}tot\text{-}int}$ values, these $U_{tot\text{-}int}$ values represent a single point on the greater uptake versus concentration kinetic curves.

[33] Fitting the M-M equation to our $U_{tot\text{-}dyn}$ data (Figure 7), we estimated maximum uptake rates (U_{max}) and half-saturation constants (K_m). Maximum uptake rates were 240 at site 2, 104 at site 3, and 65 $\mu g\ m^{-2}\ min^{-1}$ at site 4 (Table 4). The K_m values were 13.8 at site 2, 4.2 at site 3, and 14.4 $\mu g\ L^{-1}$ at site 4 (Table 4).

3.6. Results Summary

[34] In summary, physical and biological processes contributed to total NO_3-N retention over our stream reaches and along the stream network. At the 3744 m stream network scale, physical retention accounted for 81%, while biological retention accounted for 8% of total (89%) NO_3-N retention. Total retention decreased moving downstream and was 65% between sites 0 and 2, 59% between sites 2 and 3, and 21% between sites 3 and 4 (Table 2). This is largely because physical contributions to total retention reduced greatly moving downstream. Uptake lengths increased moving downstream, with the longest uptake lengths observed between sites 3 and 4 (Figure 5). Nutrient use efficiency ($V_{f\text{-}dyn}$) decreased drastically over modest nutrient concentration ranges at each sampling site (Figure 6). Also, biological retention capacity as indicated by U_{max} decreased in a downstream direction. However, because physical retention decreased to a greater extent than biological retention did, biological contributions to total retention (i.e., biological:total retention ratios) increased at downstream sites. These differential total retention capacities across stream reaches demonstrate the importance of serial nutrient processing along stream networks in controlling nutrient transport. Furthermore, biological and hydrological processes controlled total nutrient retention, which highlights the need to quantify both biological and physical retention to accurately assess stream reach and stream network nutrient export.

4. Discussion

4.1. What are the Relative Roles of Physical and Biological Processes in NO_3-N Retention?

[35] Traditional stream nutrient spiraling studies have been concerned primarily with the biological uptake of nutrients, and much recent work has shown that streams are biologically active with the capacity to affect nutrient export [*Alexander et al.*, 2000; *Bernhardt et al.*, 2003; *Bernhardt et al.*, 2005; *Peterson et al.*, 2001]. This is an important aspect of watershed nutrient retention but neglects the role that physical processes play in the retention of nutrients because traditional spiraling studies focus only on tracer recovered at the base of the study reach (but see *Runkel* [2007], *Triska et al.* [1989b]).

[36] Streams are bidirectional systems that lose and gain water to and from local groundwater as they flow downstream at spatial and temporal scales greater than typically attributed to hyporheic exchange processes [*Covino and McGlynn*, 2007]. These losses and gains impact both stream discharge and stream solute transport. We observed both gross losses and gains over each of our net gaining stream segments (Figure 3). We attribute physical retention to stream water leaving the stream and entering groundwater and/or hyporheic flow paths not sampled at the downstream BTC location on the time scale of the experiment (~5 h) [*Harvey et al.*, 1996]. Nutrient tracer that enters these alternate flow paths (i.e., water leaving the channel) may be taken up biologically outside of the stream channel (i.e., riparian plant uptake), stored in groundwater, and/or return to the channel at some point. However, each of these fates serve to delay export from the watershed and contribute to overall nutrient retention.

[37] Gross water losses observed along the stream network indicate that physical loss of tracer can occur despite net stream discharge increases (i.e., increasing discharge moving downstream) [*Payn et al.*, 2009]. Hydrologic losses were offset by gross gains of water not labeled by our tracer experiment, and thus, losses and gains represent the turnover or exchange of water in a downstream direction (i.e., not the "same" water) (in the sense of *Covino and McGlynn* [2007]). Longitudinal changes to channel morphology could explain in part the differences in physical loss that we observed. At downstream reaches, the slope decreases, velocity increases, and the stream becomes deeper and narrower (Tables 1 and 3). This changing width-to-depth ratio causes less of the channel water to be in contact with the margins of the channel. Therefore, much of the water is

traveling through a well-lubricated corridor (i.e., no interaction with the channel margins, only with other surrounding water), and the decreased slope causes less water to be forced out of the channel because of hydraulic gradients (similar to that shown by *Harvey and Bencala* [1993]). Combined, these could result in less hydrologic loss as stream size increases in these systems.

[38] Recognizing and quantifying this physical water and associated solute turnover is critical for understanding nutrient export dynamics, nutrient retention, and observed spatial and temporal stream water concentration inertia [*Brookshire et al.*, 2009; *Covino and McGlynn*, 2007]. These results suggest that hydrologic losses/gains (water turnover) can reset or buffer watershed solute signatures on short timescales through physical exchange and on long timescales through altered biogeochemical cycling in previously underappreciated flow domains. This is a critical point because most of our groundwater-surface water exchange and hyporheic understanding comes from analysis of recovered tracer only [e.g., *Bencala and Walters*, 1983; *Morrice et al.*, 1997] and has neglected exchanges on larger space-time scales (but see *Covino and McGlynn* [2007], *Triska et al.* [1989a], *Wroblicky et al.* [1998]). This simple mass balance quantification of nonrecovered tracer provides important context for understanding nutrient transport and biological uptake (i.e., interpretation of recovered tracer). It is within this framework that in-stream biological retention of nutrients should be placed to improve understanding of overall stream network control of nutrient export dynamics.

[39] Here we determined both the hydrological (i.e., physical retention) and biological components of total retention. We observed that physical retention was consistently greater than biological, often by an order of magnitude (Figure 2 and Table 2). The magnitude of physical retention varied from 13% to 58% between stream reaches and decreased moving downstream (Figure 2 and Table 2). In-stream biological uptake of NO_3-N accounted for 7%–12% of the total retention across individual stream reaches and 8% of total retention across the entire 3744 m network (Figure 2 and Table 2). Biological retention became a larger proportion of total retention moving downstream and increased from 10.8% between sites 0 and 2 to 33.3% between sites 3 and 4 (Figure 2b). This is largely due to a strong decrease in physical retention moving from upstream to downstream (Table 2). Combined physical and biological retention (i.e., total retention) of NO_3-N over the 3744 m stream network totaled 89%; only 11% of added tracer was exported beyond the study network in stream flow (Table 2). The large difference between physical (81%) and biological (8%) contributions to total retention over 3744 m of stream length suggests that physical processes can exert strong controls over watershed nutrient export in mountain systems. Research in other systems of the mountainous western United States have demonstrated the importance of these hydrologic exchanges on stream water chemistry and channel water balances [*Covino and McGlynn*, 2007; *Payn et al.*, 2009]. Since most stream nutrient spiraling research has focused only on biological uptake (recovered tracer), physical retention processes need to be incorporated into future research in other systems.

[40] Hydrologically, these results are consistent with other studies that have shown that once streams exit mountains and move across alluvial valleys they tend to lose less water (decreased groundwater interaction) [*Covino and McGlynn*, 2007] and median flow velocities tend to increase (decreased residence time) [*Wondzell et al.*, 2007]. Furthermore, complementary data from the Bull Trout Lake Watershed show that hydrologic losses from streams decrease as stream sizes increase across the full range of streams in the watershed (10–2000 L s^{-1}) (T. P. Covino et al., An approach to incorporate stream gains and losses into a stream network scale transport model, manuscript in preparation, 2010). Research from a mountain watershed in southwestern Montana also indicated that biological retention became a larger proportion of total retention moving in a downstream direction (R. A. McNamara et al., The dynamics of in-stream nitrate retention across development gradients, ambient nitrate concentrations, and stream network position in a rapidly developing mountain watershed, manuscript in preparation, 2010), and *Tank et al.* [2008] found high biotic demand for dissolved inorganic nitrogen in a large western U.S. river (7th order, 12,000 L s^{-1}). While these results only begin to elucidate the relative influence of biological and physical retention in a few western U.S. systems, they do suggest that biological processes could provide important contributions to total nutrient retention in rivers of increasing size in mountainous watersheds. Furthermore, we suggest that these findings warrant further research of the relative contributions of physical and biological retention to total retention across a broad range of landscape settings, land use types, and stream sizes to determine how these processes vary across systems and between biomes.

[41] Biological retention is strongly controlled by nutrient concentration however, and the influence of concentration on uptake efficiency must also be appreciated and quantified. An improved understanding of both biological and physical NO_3-N retention is required to ascertain and deconvolute the relative influences watershed processes exert over the integrated signals observed at the watershed outlet.

4.2. How Does Stream NO_3-N Concentration Impact Biological Retention and Stream NO_3-N Spiraling?

[42] The combination of hydrologic turnover and in-stream nutrient uptake determine overall stream nutrient spiraling dynamics. In addition to partitioning nutrient retention into physical and biological components, we also investigated the influence of stream NO_3-N concentration on biological uptake of nutrient and nutrient spiraling metrics. These analyses and resulting metrics represent integrated biological processes and nutrient use based on uptake of nutrient tracer relative to recovered conservative tracer.

[43] Within each stream reach in the network, spiraling was strongly influenced by nutrient concentration. Dynamic uptake lengths ($S_{w\text{-}add\text{-}dyn}$) increased linearly with concentration in each of our stream segments, indicative of M-M kinetics (Figure 5). While M-M kinetics were appropriate in this case study, other kinetic models (e.g., first-order, efficiency loss) may apply in other systems. For example, human impacted systems or streams with high nutrient concentrations could respond differently. Indeed, an advantage of the TASCC approach is the ability to develop spiraling-concentration curves, to determine how different streams respond to nutrient inputs, and to assign and parameterize appropriate kinetic models. In this case study

our results demonstrate decreased nutrient use efficiency with increased concentration, which has also been shown in previous studies [e.g., *Hart et al.*, 1992; *Mulholland et al.*, 2002]. The linear relationships between $S_{w\text{-}add\text{-}dyn}$ and nutrient concentration enable extrapolation to ambient concentrations under M-M assumptions to estimate $S_{w\text{-}amb}$ [*Payn et al.*, 2005] (Figure 5). An assumption in M-M experiments is that enzyme concentration remains constant, while substrate concentration is varied [*Voet and Voet*, 1995]. As such, the application of M-M kinetics to stream nutrient spiraling is appropriate in experiments where biomass remains constant while nutrient concentration is varied. This assumption is met in experiments within a stream reach where nutrient concentration is manipulated and response (i.e., uptake) is measured; however, these assumptions are not typically met for interstream comparisons and regressions of spiraling metrics versus concentration across different systems or stream reaches. But interstream comparisons can be useful to help elucidate global relationships and to understand how uptake-concentration dynamics might vary between streams of differing biomes and land use types [*Mulholland et al.*, 2008; *O'Brien et al.*, 2007].

[44] Over the stream reaches $S_{w\text{-}amb}$ ranged between 426 and 1575 m (Figure 5 and Table 4), and corresponding $V_{f\text{-}amb}$ values ranged from 3.4 to 9.3 mm min^{-1} and U_{amb} values from 19 to 58 μg m^{-2} min^{-1} (Table 4). We focus our attention on the $V_{f\text{-}amb}$ and U_{amb} results to minimize influences due to differences in discharge between the sites. Both $V_{f\text{-}amb}$, which provides a measure of uptake efficiency relative to nutrient availability [*Stream Solute Workshop*, 1990], and U_{amb} decreased moving downstream (Table 4). Our results contrast with that of *Ensign and Doyle* [2006] who found uptake velocity (V_f) increased as flow velocity increased, in their interstream comparison and suggested this was due to reduced thickness of the diffusive boundary layer. The authors further noted that differences in biological characteristics between streams complicate interstream comparisons [*Ensign and Doyle*, 2006]. Indeed, past studies in the Bull Trout Watershed show that epilithic chlorophyll a decreases longitudinally down the network, and this is associated with increased sediment mobility due in part to sediment fining [*Myers et al.*, 2007].

[45] While our results do not show similar trends as those of *Ensign and Doyle* [2006], we do agree with the authors' conclusions that larger-order streams are important to understand for network-scale nutrient export. In the Bull Trout Lake Watershed, our data indicate that the alluvial valley bottom stream segment (highest stream order in the watershed) had lower $V_{f\text{-}amb}$, U_{amb}, and U_{max}; greater median flow velocities; and less stream-groundwater exchange compared to smaller streams higher in the watershed. Given the larger $V_{f\text{-}amb}$, U_{amb}, and U_{max} values higher in the watershed and the fact that headwater streams drain by far the largest area of the earth's surface [*Freeze and Cherry*, 1979], these results support previous research that has noted the importance of small streams in watershed nutrient retention [*Peterson et al.*, 2001]. However, because there was a greater decrease in physical retention than biological retention moving downstream, biological contributions became a larger proportion of total retention as stream size increased (Figure 2b). Together, these results suggest that increased understanding of these nutrient-retention dynamics across stream sizes is necessary to interpret the integrated signals observed at watershed outlets and to improve network export models.

[46] At each of our BTC sampling sites $V_{f\text{-}tot\text{-}dyn}$ and $U_{tot\text{-}dyn}$ followed M-M kinetics (Figures 6 and 7). Both patterns show that NO_3-N was used more efficiently at lower concentrations relative to higher concentrations, as has been shown in other studies [*Dodds et al.*, 2002; *Earl et al.*, 2006; *O'Brien et al.*, 2007]. The BTC-integrated total uptake velocities ($V_{f\text{-}tot\text{-}int}$) and total uptake rates ($U_{tot\text{-}int}$) fell in the midranges of the dynamic spiraling parameter versus concentration curves and did not resemble ambient spiraling values (i.e., $V_{f\text{-}amb}$ and U_{amb} were different than $V_{f\text{-}int}$ and U_{int}) (Figures 6 and 7). Because BTC-integrated (or steady state/constant-rate) approaches produce only one data point on the greater spiraling metric-concentration curve, they provide little information regarding the relationship between uptake and concentration or how spiraling changes as concentration increases. While we applied the BTC-integrated technique to our data, we do not suggest it as the preferred method of analysis. Far more informative are data produced from the dynamic TASCC analyses and development of stream reach kinetic curves, which allow for spiraling metric characterization from ambient to saturation (Covino et al., submitted manuscript, 2010).

[47] The M-M plots of $U_{tot\text{-}dyn}$ versus concentration (Figure 7) allow quantification of U_{max} and K_m in addition to U_{amb}, providing more comprehensive information on stream uptake responses to elevated nutrients. For example, the region of each curve between U_{amb} and U_{max} is the stream response range or adaptation to increased nutrient concentration. U_{max} is the maximum biological retention rate and ranged from 240 to 65 μg m^{-2} min^{-1} decreasing in a downstream direction (Table 4). This indicates that downstream reaches became saturated at lower uptake rates than upstream reaches. Furthermore, this means that upstream reaches would retain a higher proportion of added NO_3-N and have lower fractional export if each (upstream and downstream reaches) received the same nutrient loading.

[48] K_m is the half saturation concentration or the concentration at 50% of the U_{max} uptake rate. Stream reaches with higher K_m values reach U_{max} at higher concentrations, however not necessarily at higher U_{max} uptake rates. For example, site 4 had the highest K_m (14.4 μg L^{-1}) but the lowest U_{max} (65 μg m^{-2} min^{-1}) and site 2 had the highest U_{max} and an intermediate K_m. In addition, U_{amb} is not indicative of either U_{max} or K_m and provides little insight into stream response to changing concentrations. This is demonstrated by reaches 2 and 3 that had the same U_{amb} of 58 μg m^{-2} min^{-1}, but U_{max} was 240 μg m^{-2} min^{-1} at site 2 and 104 μg m^{-2} min^{-1} at site 3, while K_m was 13.8 μg L^{-1} at site 2 and 4.2 μg L^{-1} at site 3 (Table 4). Therefore, consideration of all M-M parameters together is required to understand stream nutrient biological retention dynamics. U_{amb} reflects uptake for background environmental conditions, while reaches with higher U_{max} values have greater retention capacity. However, if two reaches have comparable U_{max}, then the reach with the lower K_m has greater retention capacity because it reaches U_{max} more quickly. The shape of the M-M curve is reflected in these three key parameters that together describe stream reach uptake characteristics.

[49] Similar results are displayed in terms of uptake efficiency in the plot of $V_{f\text{-}tot\text{-}dyn}$ versus nutrient concentration (Figure 6). Specifically, that efficiency of nutrient use reduced drastically over a range of ~100–150 μg L^{-1} NO_3-N (Figure 6). This suggests that streams in the Bull Trout Lake Watershed, and other similar streams, may become very inefficient in N usage over modest concentration ranges. *Earl et al.* [2006] similarly found that streams may pass through various stages of N saturation with small increases in concentration. Although each of our sites began at very different nutrient uptake efficiency (i.e., $V_{f\text{-}tot\text{-}dyn}$) values, each decreased to values of ~1–2 mm min^{-1} at concentrations greater than 100 μg L^{-1} (Figure 6). Therefore, even stream segments that have very high nutrient usage efficiencies under ambient conditions may become inefficient and near saturated with increases as little as ~100 μg L^{-1}. The intersection of seasonal (i.e., temperature, biomass) and concentration influences on biological uptake partially control nutrient use efficiency and watershed export and warrant further attention. For example, high nutrient concentrations that can occur during spring runoff in snowmelt driven systems will likely lead to decreased use efficiencies, which combined with cold stream water temperatures, and high Q could potentially cause a large proportion of nutrients to be exported and contribute to increased downstream loading. Furthermore, the relative contributions of physical and biological retention to total nutrient retention will vary seasonally [see *Hall et al.*, 2009] and will be controlled by the combination of (among other things) hydrologic characteristics (e.g., discharge, median flow velocity, gross gain/loss), nutrient concentration, biomass, and stream water temperature and their interactions will ultimately determine watershed nutrient export.

[50] The variability of reach response to nutrient loading and concentration even within the same network or between adjacent reaches is critical to consider in the context of network nutrient export models or cross-site comparison. For example, within a stream reach, nutrient uptake efficiency is strongly influenced by upstream loading (i.e., concentration), which in turn controls downstream export, and so on. *Alexander et al.* [2009] noted substantial decreases in nitrate removal (i.e., denitrification) at times and/or places where high nutrient loading occurred, and *Mulholland et al.* [2008] noted that the relationship between use efficiency and concentration needs to be addressed in order to improve network export models and estimates of downstream loading. Dynamic uptake curves for a given reach represent modification of upstream nutrient loading accomplished by a reach as it transforms upstream input to downstream export. Therefore, the M-M curve (or other appropriate kinetic model curve) can be used diagnostically or in a forward sense in stream nutrient export models. We also suggest that physical retention be incorporated. The interactions between physical retention, serial processing, nutrient uptake efficiency (i.e., uptake kinetic curves), and their combined effects should be included in nutrient transport models to understand the role of the stream network in modifying downstream transport and watershed export.

4.3. Summary: Incorporating Stream Gains and Losses and Spiraling-Concentration Relationships to Understand Stream Nitrogen Transport

[51] Stream gains and losses have been noted as important in setting stream water chemistry [*Covino and McGlynn*, 2007] and in-stream water balances and water turnover. Here our data suggest that these processes, and ensuing physical nutrient retention, may also be important controls over watershed nutrient export. However, physical retention is not often considered in stream nutrient spiraling studies. Previous studies of in-stream nutrient spiraling generally considered nutrient retention relative to only recovered conservative tracer. This approach provides information regarding the biological component of nutrient retention but neglects physical retention of water/tracer. Here we have shown that gross loss of tracer can occur in net gaining streams and stream reaches. Therefore, it cannot be assumed that net gaining or net losing streams are only gaining or losing across the reach. Although physical retention was greater than biological retention across each of our successive stream reaches, proportional biological contributions to total retention increased in a downstream direction. These results suggest that physical retention may be important in headwater streams and biological contributions may become a larger percentage of total retention with increased stream size, particularly in mountain systems. Because total retention is composed of both physical and biological components, it is important that future nutrient spiraling research quantify both of these important aspects of watershed nutrient retention and export. Furthermore, future research to quantify both of these retention processes in systems other than the watershed we present here will help to elucidate how physical and biological components interact to control overall export across the spectrum of stream and watershed types.

[52] Biological uptake and associated stream spiraling metrics were strongly controlled by nutrient concentration in each of our stream reaches, and nutrient uptake (e.g., U_{amb} and U_{max}) was greater in the watershed highlighting the importance of small streams in nutrient retention [e.g., *Peterson et al.*, 2001]. The relationships between spiraling metrics and nutrient concentration followed M-M kinetics; however, other kinetic models may apply in other systems (e.g., first-order, efficiency loss). These relationships indicated that nutrient uptake efficiencies decreased with elevated nutrient concentrations. Furthermore, uptake efficiencies decreased drastically over modest concentration ranges of ~100 μg NO_3-N (Figures 6 and 7). Among stream reaches, both U_{amb} and biological nutrient retention capacity as indicated by U_{max} decreased in a downstream direction. Together, our results indicated that the stream reaches with the highest relative biological contribution to total retention actually had lower biological uptake capacities. Thus, the relationships between biological, physical, and total retention are important to understand for assessing network nutrient export. Furthermore, these results indicate that for a given nutrient load, biological response to that load varies between stream reaches. Therefore, we suggest that it is not only important to understand how concentration influences uptake within a stream reach, but also how these relationships vary across the landscape.

[53] An inherent aspect of streams and stream networks is downstream transport. In a stream network sense, the output from one stream reach becomes the input for the next. The shape of the uptake-concentration curve for each stream reach characterizes in-stream biological uptake of nutrient, and combined with hydrologic turnover (i.e., physical retention), both will control nutrient export to the next reach in the network. The implication is that position within the network and network organization or topology is important. Specifically, the arrangement of stream reaches, each with associated hydrologic (physical retention) and uptake kinetic characteristics, will integrate to control serial processing efficacy and overall watershed retention and export. Coupled understanding of hydrologic turnover and spiraling-concentration dynamics is critical to assessing, modeling, and predicting watershed and stream network response to NO_3-N loading and subsequent export to downstream communities. We suggest these relationships be studied across landscape scales and land use types to better understand the physical and biological components of nutrient retention across the stream network continua.

[54] **Acknowledgments.** Financial support was provided by grants from the National Science Foundation DEB-0519264 (to Montana State University) and DEB 0519327 (to Utah State University) and an Environmental Protection Agency (EPA) STAR Fellowship awarded to Covino. We would like to thank Chelsea Crenshaw, Maury Valett, and Steven Thomas for discussions regarding this work; Ian Washbourne for laboratory analysis; and Meg Kline and Mark Schaeffer for help collecting field data. We thank the Boise National Forest for allowing access to sampling sites.

References

Alexander, R. B., R. A. Smith, and G. E. Schwarz (2000), Effect of stream channel size on the delivery of nitrogen to the gulf of mexico, *Nature*, *403*, 758–761.

Alexander, R. B., J. K. Bohlke, E. W. Boyer, M. B. David, J. W. Harvey, P. J. Mulholland, S. P. Seitzinger, C. R. Tobias, C. Tonitto, and W. M. Wollheim (2009), Dynamic modeling of nitrogen losses in river networks unravels the coupled effects of hydrological and biogeochemical processes, *Biogeochemistry*, *93*, 91–116.

Arp, C. D., and M. A. Baker (2007), Discontinuities in stream nutrient uptake below lakes in mountain drainage networks, *Limnol. Oceanogr.*, *52*, 1978–1990.

Baker, M. A., C. N. Dahm, and H. M. Valett (1999), Acetate retention and metabolism in the hyporheic zone of a mountain stream, *Limnol. Oceanogr.*, *44*, 1530–1539.

Bencala, K. E., and R. A. Walters (1983), Simulation of solute transport in a mountain pool-and-riffle stream - a transient storage model, *Water Resour. Res.*, *19*, 718–724.

Bernhardt, E. S., G. E. Likens, D. C. Buso, and C. T. Driscoll (2003), In-stream uptake dampens effects of major forest disturbance on watershed nitrogen export, *Proc. Natl. Acad. Sci. USA*, *100*(18), 10,304–10,308.

Bernhardt, E. S., et al. (2005), Can't see the forest for the stream?: In-stream processing and terrestrial nitrogen exports, *Bioscience*, *55*, 219–230.

Bormann, F. H., and G. E. Likens (1967), Nutrient cycling, *Science*, *155*, 424–429.

Brookshire, E. N. J., H. M. Valett, S. A. Thomas, and J. R. Webster (2005), Coupled cycling of dissolved organic nitrogen and carbon in a forest stream, *Ecology*, *86*, 2487–2496.

Brookshire, E. N., H. M. Valett, and S. Gerber (2009), Maintenance of terrestrial nutrient loss signatures during in-stream transport, *Ecology*, *90*, 293–299.

Covino, T. P., and B. L. McGlynn (2007), Stream gains and losses across a mountain to valley transition: Impacts on watershed hydrology and stream water chemistry, *Water Resour. Res.*, *43*, W10431, doi:10.1029/2006WR005544.

Covino, T. P., B. L. McGlynn, and R. A. McNamara (2010), Tracer additions for spiraling curve characterization (TASCC): Quantifying stream nutrient uptake kinetics from ambient to saturation, *Limnol. Oceanogr. Methods*, in press.

Dent, C. L., and N. B. Grimm (1999), Spatial heterogeneity of stream water nutrient concentrations over successional time, *Ecology*, *80*, 2283–2298.

Dodds, W. K., et al. (2002), N uptake as a function of concentration in streams, *J. North Am. Benthol. Soc.*, *21*(2), 206–220.

Earl, S. R., H. M. Valett, and J. R. Webster (2006), Nitrogen saturation in stream ecosystems, *Ecology*, *87*, 3140–3151.

Ensign, S. H., and M. W. Doyle (2006), Nutrient spiraling in streams and river networks, *J. Geophys. Res.*, *111*, G04009, doi:10.1029/2005JG000114.

Freeze, R. A., and J. A. Cherry (1979), *Groundwater*, 1st ed., 604 pp., Prentice-Hall, Englewood Cliffs, NJ.

Hall, R. O., M. A. Baker, C. D. Arp, and B. J. Koch (2009), Hydrologic control of nitrogen removal, storage, and export in a mountain stream, *Limnol. Oceanogr.*, *54*, 2128–2142.

Hart, B. T., P. Freeman, and I. D. McKelvie (1992), Whole-stream phosphorus release studies - variation in uptake length with initial phosphorus concentration, *Hydrobiologia*, *235*, 573–584.

Harvey, J. W., and K. E. Bencala (1993), The effect of streambed topography on surface-subsurface water exchange in mountain catchments, *Water Resour. Res.*, *29*, 89–98, doi:10.1029/92WR01960.

Harvey, J. W., B. J. Wagner, and K. E. Bencala (1996), Evaluating the reliability of the stream tracer approach to characterize stream-subsurface water exchange., *Water Resour. Res.*, *32*, 2441–2451, doi:10.1029/96WR01268.

Kiilsgaard, T., L. Stanford, and R. Lewis (2003), Preliminary geologic map of the northesat part of the deadwood river 30 x 60 minute quadrangle, idaho, *Idaho Geologic Survey*.

Morrice, J. A., H. M. Valett, C. N. Dahm, and M. E. Campana (1997), Alluvial characteristics, groundwater–surface water exchange and hydrological retention in headwater streams, *Hydrol. Process.*, *11*, 253–267.

Mulholland, P. J., et al. (2002), Can uptake length in streams be determined by nutrient addition experiments? Results from an interbiome comparison study, *J. North Am. Benthol. Soc.*, *21*(4), 544–560.

Mulholland, P. J., et al. (2008), Stream denitrification across biomes and its response to anthropogenic nitrate loading, *Nature*, *452*, 202–246.

Mulholland, P. J., et al. (2009), Nitrate removal in stream ecosystems measured by n-15 addition experiments: Denitrification, *Limnol. Oceanogr.*, *54*, 666–680.

Myers, A. K., A. M. Marcarelli, C. D. Arp, M. A. Baker, and W. A. Wurtsbaugh (2007), Disruptions of stream sediment size and stability by lakes in mountain watersheds: Potential effects on periphyton biomass, *J. North Am. Benthol. Soc.*, *26*, 390–400.

Newbold, J. D., J. W. Elwood, R. V. Oneill, and W. Vanwinkle (1981), Measuring nutrient spiralling in streams, *Can. J. Fish. Aquat. Sci.*, *38*, 860–863.

Newbold, J. D., J. W. Elwood, R. V. Oneill, and A. L. Sheldon (1983), Phosphorus dynamics in a woodland stream ecosystem - a study of nutrient spiralling, *Ecology*, *64*, 1249–1265.

Newbold, J. D., T. L. Bott, L. A. Kaplan, C. L. Dow, J. K. Jackson, A. K. Aufdenkampe, L. A. Martin, D. J. Van Horn, and A. A. de Long (2006), Uptake of nutrients and organic c in streams in new york city drinking-water-supply watersheds, *J. North Am. Benthol. Soc.*, *25*, 998–1017.

O'Brien, J. M., W. K. Dodds, K. C. Wilson, J. N. Murdock, and J. Eichmiller (2007), The saturation of n cycling in central plains streams: N-15 experiments across a broad gradient of nitrate concentrations, *Biogeochemistry*, *84*, 31–49.

Payn, R. A., J. R. Webster, P. J. Mulholland, H. M. Valett, and W. K. Dodds (2005), Estimation of stream nutrient uptake from nutrient addition experiments, *Limnol. Oceanogr.*, *3*, 174–182.

Payn, R. A., M. N. Gooseff, B. L. McGlynn, K. E. Bencala, and S. M. Wondzell (2009), Channel water balance and exchange with subsurface flow along a mountain headwater stream in montana, united states, *Water Resour. Res.*, *45*, W11427, doi:10.1029/2008WR007644.

Peterson, B. J., et al. (2001), Control of nitrogen export from watersheds by headwater streams, *Science*, *292*(5514), 86–90.

Royer, T. V., J. L. Tank, and M. B. David (2004), Transport and fate of nitrate in headwater agricultural streams in illinois, *J. Environ. Qual.*, *33*, 1296–1304.

Ruggiero, A., A. G. Solimini, M. Anello, A. Romano, M. De Cicco, and G. Carchini (2006), Nitrogen and phosphorus retention in a human altered stream, *Chem. Ecol.*, *22*, S1–S13.

Runkel, R. L. (2007), Toward a transport-based analysis of nutrient spiraling and uptake in streams, *Limnol. Oceanogr.*, *5*, 50–62.

Stream Solute Workshop (1990), Concepts and methods for assessing solute dynamics in stream ecosystems, *J. North Am. Benthol. Soc.*, *9*, 95–119.

Tank, J. L., E. J. Rosi-Marshall, M. A. Baker, and R. O. Hall (2008), Are rivers just big streams? A pulse method to quantify nitrogen demand in a large river, *Ecology*, *89*, 2935–2945.

Triska, F. J., V. C. Kennedy, R. J. Avanzino, G. W. Zellweger, and K. E. Bencala (1989a), Retention and transport of nutrients in a 3rd-order stream in northwestern california - hyporheic processes, *Ecology*, *70*, 1893–1905.

Triska, F. J., V. C. Kennedy, R. J. Avanzino, G. W. Zellweger, and K. E. Bencala (1989b), Retention and transport of nutrients in a 3rd-order stream - channel processes, *Ecology*, *70*, 1877–1892.

Voet, D., and J. Voet (1995), *Biochemistry*, 2nd ed., 1361 pp., John Wiley and Sons, Inc., New York.

Webster, J. R., and B. C. Patten (1979), Effects of watershed perturbation on stream potassium and calcium dynamics, *Ecol. Monogr.*, *49*, 51–72.

Wondzell, S. M., M. N. Gooseff, and B. L. McGlynn (2007), Flow velocity and the hydrologic behavior of streams during baseflow, *Geophys. Res. Lett.*, *34*, L24404, doi:10.1029/2007GL031256.

Wroblicky, G. J., M. E. Campana, H. M. Valett, and C. N. Dahm (1998), Seasonal variation in surface-subsurface water exchange and lateral hyporheic area of two stream-aquifer systems, *Water Resour. Res.*, *34*, 317–328, doi:10.1029/97WR03285.

M. Baker, Utah State University, Logan, UT, USA.

T. Covino and B. McGlynn, Montana State University, 334 Leon Johnson Hall, Bozeman, MT 59717, USA. (tpcovino@gmail.com)